npj | Quantum Materials

www.nature.com/npjquantmats

Corrected: Author correction

ARTICLE OPEN

Unconventional and conventional quantum criticalities in $CeRh_{0.58}Ir_{0.42}In_5$

Yongkang Luo[1], Xin Lu[2], Adam P. Dioguardi[1], Priscila S. F. Rosa[1], Eric D. Bauer[1], Qimiao Si[3] and Joe D. Thompson[1]

An appropriate description of the state of matter that appears as a second order phase transition is tuned toward zero temperature, viz. quantum-critical point (QCP), poses fundamental and still not fully answered questions. Experiments are needed both to test basic conclusions and to guide further refinement of theoretical models. Here, charge and entropy transport properties as well as AC specific heat of the heavy-fermion compound $CeRh_{0.58}Ir_{0.42}In_5$, measured as a function of pressure, reveal two qualitatively different QCPs in a *single* material driven by a single non-symmetry-breaking tuning parameter. A discontinuous sign-change jump in thermopower suggests an unconventional QCP at p_{c1} accompanied by an abrupt Fermi-surface reconstruction that is followed by a conventional spin-density-wave critical point at p_{c2} across which the Fermi surface evolves smoothly to a heavy Fermi-liquid state. These experiments are consistent with some theoretical predictions, including the sequence of critical points and the temperature dependence of the thermopower in their vicinity.

npj Quantum Materials (2018)3:6 ; doi:10.1038/s41535-018-0080-9

INTRODUCTION

Heavy-fermion metals have emerged as prototypes for discovering quantum-critical states[1,2] that are of broad interest as they are believed to be the origin of non-Fermi-liquid (NFL) and unconventional superconducting (SC) phases in classes of strongly correlated electron materials, ranging from organics to metallic oxides. Generically, a QCP is an end point at absolute zero temperature of a continuous transition that separates ordered and disordered phases and is accessed by a non-thermal control parameter g, such as chemical doping (x), pressure (p) and magnetic field (B).[3,4] The conventional model of quantum criticality is based on a quantum extension of the Landau–Ginzburg–Wilson theory of classical, thermally-driven phase transitions and considers only fluctuations of a spin-density-wave (SDW) order parameter.[4] In this model, which does not treat electronic degrees of freedom as part of the critical excitations, the Fermi surface (FS) evolves smoothly as a function of g across the QCP.[5,6] Though this model provides a reasonable account of physical properties in some systems near a QCP,[4] it fails fundamentally to describe critical responses in other metallic systems in which there is accumulating evidence for unconventional quantum criticality, most notably in heavy-fermion compounds.[7–13] Alternatives to the conventional model, frequently called local, selective Mott or Kondo-breakdown theories, invoke criticality of electronic degrees of freedom that may be concurrent with magnetic criticality,[1,2,14,15] and the QCP is accompanied by a sharp reconstruction of the FS. These models of criticality are unconventional in that they go beyond the Landau–Ginzburg–Wilson framework. Though there is experimental support for them,[7–13] the concept of fluctuations of a symmetry-breaking order parameter with qualitative reconstruction of electronic states requires further theoretical understanding. For progress, it is important for experiments to both test their basic conclusions, such as the evolution of the FS across the QCP, and to guide their further development.

The critical state that develops near the $T = 0$ magnetic/non-magnetic boundary as a function of x in heavy-fermion $CeCu_{6-x}Au_x$ motivated early models of unconventional QCPs under applied pressure or magnetic field.[7] Similar to $CeCu_{6-x}Au_x$ under applied pressure and magnetic field,[16] two very different critical states are realized in $CeRhIn_5$ when different tuning parameters are used to access its QCPs. Applying pressure to $CeRhIn_5$ induces in the limit $T \to 0$ a magnetic/non-magnetic transition at a critical pressure $P_2 = 2.4$ GPa,[17–19] where deHaas-vanAlphen (dHvA) measurements find an abrupt change from small-to-large FSs and strong enhancement of the quasiparticle effective mass,[20] characteristic of an unconventional QCP. In the absence of an applied magnetic field, these responses are hidden by a dome of superconductivity (SC) that also encompasses a range of lower pressures where antiferromagnetic (AFM) order and SC coexist. At atmospheric pressure but as a function of magnetic field, which unlike pressure breaks time-reversal symmetry, there is a small-to-large FS reconstruction near 30 T within an AFM phase[21,22] that terminates in a SDW-type QCP at ~50 T.[21]

The evolution of magnetism and SC in the homologous series $CeRh_{1-x}Ir_xIn_5$ as a function of Ir content x is somewhat similar to $CeRhIn_5$ under pressure. For $x < 0.3$, there is only large-moment, incommensurate AFM order at $\mathbf{Q} = (0.5, 0.5, \sim 0.297)$,[23] and for $0.3 < x < 0.6$, an additional small-moment, commensurate (0.5, 0.5, 0.5) AFM order develops and coexists with SC.[24] At higher Ir concentrations, there is only SC.[25,26] Interestingly, as in $CeRhIn_5$ under pressure,[27] the appearance of SC in $CeRh_{1-x}Ir_xIn_5$ coincides with a change of magnetic structure,[24] making the similarity between these two cases even stronger. dHvA measurements show that the cyclotron frequencies are larger in $CeIrIn_5$ than in $CeRhIn_5$,[28] which implies that cerium's 4*f* electron participates in

[1]Los Alamos National Laboratory, Los Alamos, NM 87545, USA; [2]Center for Correlated Matter and Department of Physics, Zhejiang University, Hangzhou 310058, China and [3]Department of Physics and Astronomy and Center for Quantum Materials, Rice University, Houston, TX 77005, USA
Correspondence: Yongkang Luo (mpzslyk@gmail.com) or Joe D. Thompson (jdt@lanl.gov)

Received: 9 July 2017 Revised: 4 January 2018 Accepted: 15 January 2018
Published online: 15 February 2018

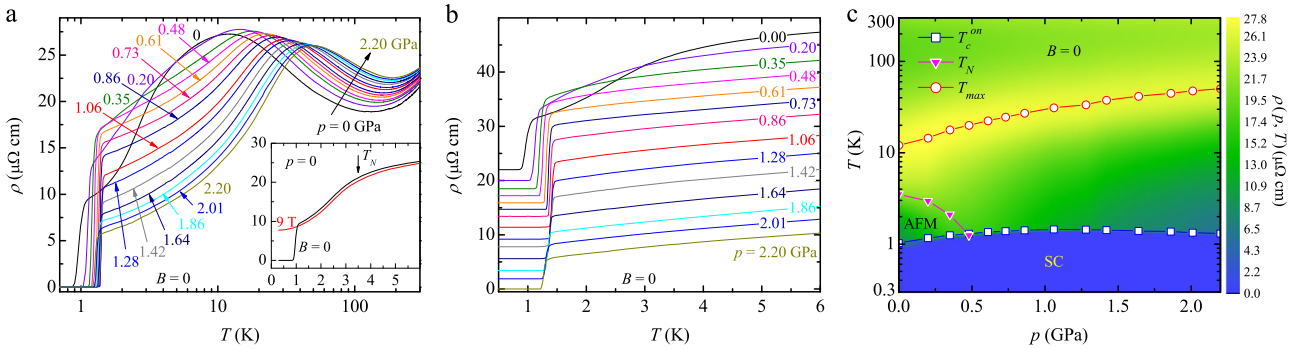

Fig. 1 Resistivity of $CeRh_{0.58}Ir_{0.42}In_5$ under pressure. **a** Temperature-dependent resistivity of $CeRh_{0.58}Ir_{0.42}In_5$ under different pressures. The inset is a comparison of $\rho(T)$ for $B = 0$ and 9 T at ambient pressure. **b** A zoom-in view of the low temperature region; the curves have been vertically shifted for clarity. **c** A contour plot constructed from $\rho(p, T)$ at zero magnetic field. Symbols show the evolution of resistivity maximum T_{max}, Néel temperature T_N and superconducting onset temperature T_c^{on}

making the larger FSs of $CeIrIn_5$ but is localized in $CeRhIn_5$. Somewhere in the $CeRh_{1-x}Ir_xIn_5$ series, there should be a change in 4*f*-electron localization and a magnetic QCP. Unfortunately, dHvA measurements have not been possible across the series. To explore these issues, we have measured the effect of pressure on the resistivity, thermopower and AC specific heat of a crystal of $CeRh_{0.58}Ir_{0.42}In_5$ whose nominal composition places it close to the critical Ir concentration $x_c \simeq 0.6$[26] where the magnetic boundary drops rapidly towards $T = 0$ at atmospheric pressure.[24] As will be discussed, these experiments reveal signatures that point to two distinct types of criticality as a function of a single, non-symmtery-breaking tuning parameter, pressure, and provide an important test of some theoretical predictions.

RESULTS

Figure 1a shows the temperature dependence of in-plane resistivity of $CeRh_{0.58}Ir_{0.42}In_5$ at pressures up to 2.20 GPa. At ambient pressure, $\rho(T)$ initially decreases upon cooling but starts to increase below 135 K and forms a pronounced broad peak around $T_{max} = 12$ K, characteristic of the onset of coherent Kondo scattering. Below T_{max}, $\rho(T)$ decreases monotonically, and the sample becomes a superconductor with an onset critical temperature $T_c^{on} = 1.04$ K. Above T_c^{on}, an inflection in $\rho(T)$ near $T_N = 3.5$ K reflects a reduction of spin-scattering due to the formation of long-range AFM order of Ce moments.[24–26,29] Under pressure, (1) T_{max} increases monotonically and reaches ~50 K at 2.20 GPa; (2) T_c^{on} increases with pressure and reaches a maximum of 1.45 K at $p = 1.06$ GPa before it starts to decrease (Fig. 1b); and, (3) the AFM order is gradually suppressed and becomes unresolvable when $p > 0.48$ GPa where the resistive anomaly is concealed by SC.

The zero-field pressure-temperature phase diagram of $CeRh_{0.58}Ir_{0.42}In_5$, constructed from resistivity measurements, is summarized in Fig. 1c where we see that evidence for magnetic order (T_N) disappears near 0.48 GPa below a dome of SC. A field of 9 T completely suppresses SC but has a negligible effect on the Néel temperature and the temperature dependence of resistivity (inset to Fig. 1a), implying that no significant magnetic-structure or Fermi-surface change is induced by this modest field. In this field, however, a resistive signature for an AFM transition continues to pressures $p > 0.48$ GPa (Fig. 2a). This evolution is seen more clearly in $d\rho/dT$ that is plotted in Fig. 2b. At ambient pressure, $d\rho/dT$ peaks near 2.5 K, which is much lower than the Néel temperature $T_N \approx 3.5$ K. From magnetic neutron diffraction on a sample with Ir content near $x = 0.42$, large-moment incommensurate antiferromagnetism develops at 3.5 K and coexisting small-moment, commensurate AFM appears below 2.7 K.[24] Specific heat measurements on our crystal in zero field (left inset to Fig. 2b) find an inflection point in C/T at 3.5 K and a peak near 2.5 K, mimicking the features in $d\rho/dT$. We, therefore, identify the inflection temperature in $d\rho/dT$ with the onset of incommensurate AFM and the peak as an approximation to the appearance of commensurate order. Applying a 9-T magnetic field retains these anomalies in C/T, showing that two magnetic transitions persist with nearly identical ordering temperatures as at zero field (right inset in Fig. 2b). It is obvious from inspection of the $d\rho/dT$ curves that they narrow quickly with increasing pressure and that for $0.61 \leq p < 1.06$ GPa the peak position changes much more slowly. At 1.06 GPa, $d\rho/dT$ approaches a constant at low temperatures, signaling that $\rho(T)$ at this pressure is almost a linear function of temperature and that a well-defined signature for an AFM transition has disappeared. This is seen more clearly in the inset to Fig. 2a where $\rho(T)$ at 1.06 GPa is essentially T-linear below about 0.75 K and there is no detectable evidence for an AFM transition.

In the right inset to Fig. 2b, we display the results of AC calorimetry (C_{ac}) measurements on the same crystal but from a separate pressure run. At 0.38 GPa, signatures of both AFM and SC transitions can be identified from the temperature dependence of C_{ac}/T at zero field, and the latter is washed out in the presence of $B = 9$ T, consistent with resistivity measurements. For $p = 0.79$ GPa and zero field, only the SC transition is visible, but when a 9-T magnetic field is turned on and SC is completely suppressed, there is kink in C_{ac}/T near 0.76 K, as in $CeCu_{(6-x)}Au_x$,[16] that reflects an AFM transition that also is evident in $d\rho/dT$ for $0.61 < p < 1.06$ GPa. Indeed, this small anomaly in C_{ac}/T disappears when pressure reaches 1.09 GPa. These specific heat and resistivity results suggest that this magnetic order, hidden by SC at zero field, is of bulk nature, and that a quantum criticality is approached near 1.06 GPa.

Further evidence for criticality comes from fitting the resistivity $\rho(T)$ to a power law:

$$\rho(T) = \rho_0 + \Delta\rho(T) = \rho_0 + AT^n, \quad (1)$$

where ρ_0 is the residual resistivity. As also shown in the inset to Fig. 2a, the low-temperature resistivity at 2.20 GPa follows a quadratic temperature dependence below about 1 K and is typical of a Fermi liquid. We take this pressure as a reference for normalizing lower pressure data in the false-color contour plot in Fig. 2c. In the low-temperature limit, this plot shows that the residual resistivity peaks near 0.6 GPa, and this is characteristic of scattering amplified by quantum fluctuations, see also Fig. 2e. In Fig. 2c, colored solid triangles denote T_N, the temperature from Fig. 2b where large-moment incommensurate AFM develops. The coincidence of strongest scattering and an extrapolation of this Néel temperature to $T = 0$ suggests that there is a quantum-phase transition of this order near $p_{c1} = 0.6$ GPa. This conclusion is supported further by the pressure-induced collapse of the broad

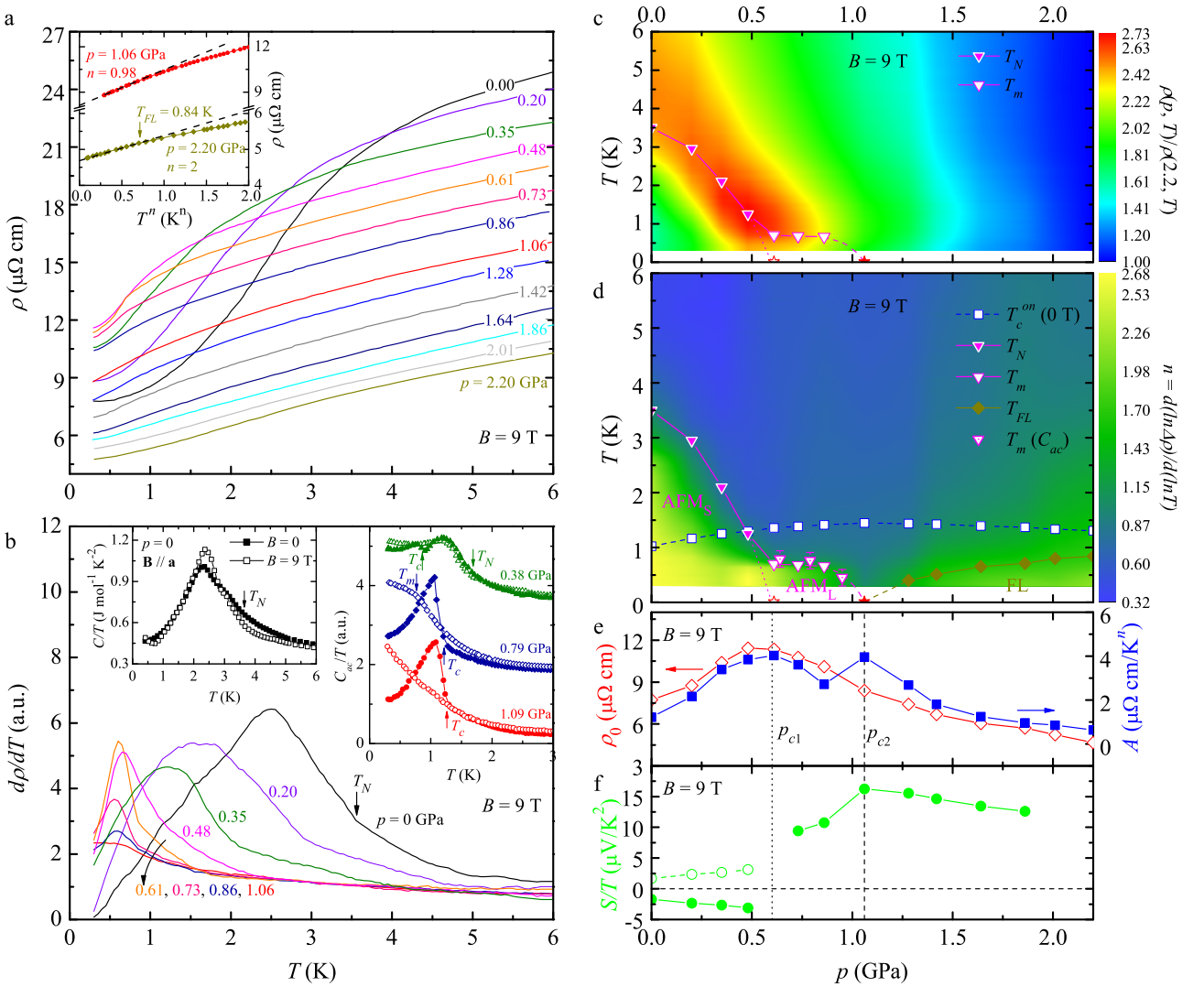

Fig. 2 Transport properties of $CeRh_{0.58}Ir_{0.42}In_5$ at $B = 9$ T, **B**||**a**. **a** $\rho(T)$ profiles at various pressures (data vertically shifted). The inset shows evidence for NFL and FL behaviors for $p = 1.06$ and 2.20 GPa, respectively. **b** dρ/dT for small applied pressures. The $\rho(T)$ data have been interpolated and three-point smoothed before differentiation. The left inset is the temperature-dependent specific heat divided by temperature (C/T) measured at $p = 0$ for fields of 0 (solid) and 9 T (open). The upturn of C/T below 0.7 K for 9 T is due to the In nuclear Schottky anomaly. The right inset plots AC calorimetry (C_{ac}/T) measured at 0.38, 0.79 and 1.09 GPa. The solid (open) symbols represent for $B = 0$ (9 T). **c** Contour plot of isothermal resistivity normalized by the resistivity at 2.2 GPa, $\rho(p, T)/\rho(2.20, T)$. **d** False contour plot of the local exponent $n = $ d ln($\Delta\rho$)/d ln(T) defined in Eq. (1). Symbols are defined in the legend and correspond to the properties obtained at 9 T, except for T_c^{on}. T_m defined from AC calorimetry is also shown. **e** The residual resistivity ρ_0 (left axis) and coefficient A (right axis). **f** The initial slope of thermopower, S/T, as a function of p; the open circles denote the absolute values for $p < 0.6$ GPa

maximum in dρ/dT to a much narrower peak at 0.61 GPa. Nevertheless, the narrow peak persists to 1.06 GPa, indicating that another magnetic transition remains to this higher pressure. As we will demonstrate, magnetic order in this pressure range is a SDW, but neutron diffraction or nuclear quadrupole resonance (NQR) experiments are needed to determine the detailed nature of this order. Irrespective of the precise nature of the magnetism, the important point is that it exists in this pressure range and we label this magnetic transition T_m. Figure 2d presents a contour plot of the local exponent n as a function of p and T. Here, n is derived from the local derivative, $n = $ d(ln $\Delta\rho$)/d(ln T). Though the residual resistivity is a maximum near 0.6 GPa, there is only a limited temperature range above this pressure where the resistivity exhibits NFL behavior with $n \sim 1.0$. This may be due to the presence of magnetism below T_m. In contrast, residual scattering is not so enhanced but there is an extended temperature range with $n \sim 1.0$ around $p_{c2} = 1.06$ GPa where T_c^{on} in zero field is a maximum. Interestingly, there is a substantially increased inelastic scattering rate manifested by peaks in the A coefficient at both p_{c1} and p_{c2} (see Fig. 2e). The maxima of A are about 4 $\mu\Omega$·cm/K^n, comparable to that in $CeRhIn_5$ at P_2,[30] indicating that the effective-mass enhancements are similar in these two systems. This comparison is shown in Fig. S1 and discussed further in the Supplementary Information (SI).

The apparent dichotomy of signatures for quantum criticality at p_{c1} and p_{c2} is a first indication that these QCPs may be different in character, and this is further supported through thermopower measurements. The thermopower is given by[31]

$$S \equiv \frac{\alpha}{\sigma} = \frac{\pi^2}{3}\frac{k_B^2 T}{q}\frac{\partial \ln \sigma(\varepsilon)}{\partial \varepsilon}\bigg|_{\varepsilon=\varepsilon_F}, \quad (2)$$

where k_B is Boltzman's constant, q is the charge of carriers, σ is the electrical conductivity, α is the Peltier conductivity, and ε_F is the chemical potential at $T = 0$. Being the energy-derivative of ln $\sigma(\varepsilon)$, S

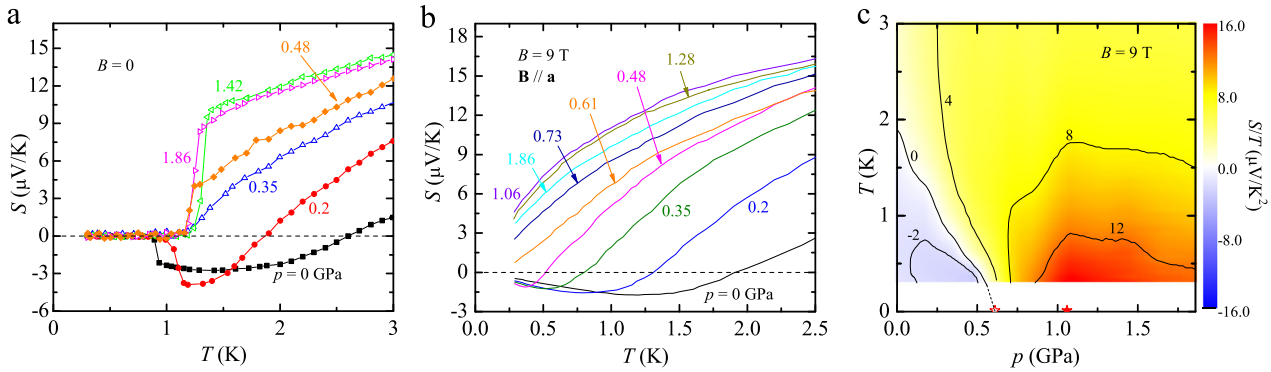

Fig. 3 Thermopower of $CeRh_{0.58}Ir_{0.42}In_5$. Temperature dependence of thermopower under various pressures, measured at zero magnetic field (**a**) and 9 T (**b**). **c** Contour plot of S/T ($B = 9$ T) as a function of p and T. The boundary where $S/T = 0$ extrapolates to near p_{c1}

is more sensitive to the Fermi-surface topology than σ. Moreover, because the entropy current $J_S = \frac{1}{T} a \cdot E$ (E is electric field), thermopower provides a measure of transport entropy per each conduction carrier.

Figure 3a displays the temperature dependence of in-plane thermopower at selected pressures without an external magnetic field. Below T_c^{on}, $S(T)$ drops to 0, demonstrating an entropy-less SC ground state. S changes sign from negative to positive near 2.6 K at $p = 0$. With applied pressure, the temperature where the sign change occurs moves to lower temperatures, and at $p = 0.35$ GPa, it coincides with T_c^{on}. Application of a 9-T field allows tracking the sign changes to lower temperatures, as shown in Fig. 3b. At $p =$ 0.61 GPa, $S(T)$ remains positive down to 0.3 K, the base temperature of our measurements, but may become negative at even lower temperature. Additional measurements to lower temperatures would be useful to determine the sign of S especially around this pressure. Irrespective of some uncertainty of $S(T)$ below 0.3 K, a sign change of thermopower with pressure seems inescapable (Fig. 3c). A smooth extrapolation of $S(T)$ suggests that $S(T)$ remains positive to $T \to 0$ when $p \geq 0.73$ GPa. The initial slope of $S(T)$ at our lowest temperatures is plotted in Fig. 2f as a function of p. There are two notable features: a discontinuous jump in S/T near p_{c1} and a maximum at p_{c2}. With S being sensitive to Fermi-surface topology, the jump in S/T implies a qualitative change in electronic properties at p_{c1}.

The temperature dependence of S/T around p_{c1} and p_{c2} is displayed in Fig. 4a,b. For $p < p_{c1}$, e.g., 0.48 GPa, S/T initially increases with decreasing T and forms a broad peak before dropping sharply as $T \to 0$. The maximum and sharp drop in S/T move to lower temperatures for $p = 0.61$ GPa, but at a slightly higher pressure (0.73 GPa), S/T increases monotonically with decreasing temperature and tends to saturate to a finite value as T approaches zero. In contrast to the asymmetry around p_{c1}, S/T approaches $T = 0$ symmetrically about p_{c2}. To the extent that S/T also is proportional to the Sommerfeld coefficient of specific heat γ in a multi-band system,[32] this temperature evolution of S/T around p_{c2} is a clear signature of quantum criticality, as discussed in the following section.

DISCUSSION

Before comparing these observations to theoretical predictions of quantum criticality, we consider possible alternative interpretations for the abrupt jump and sign change of S/T around p_{c1}. These possibilities include: (1) a change in crystal fields, (2) magnetic breakdown, (3) a valence transition and (4) and a Lifshitz transition. The crystal-field ground state of the $CeRh_{1-x}Ir_xIn_5$ series is a Γ_7 for all compositions[33] and the energy difference between ground and first-excited states only *decreases* slightly from 6.9 meV in $CeRhIn_5$ to 6.7 meV in $CeIrIn_5$.[34] It is highly improbable that a pressure of only 0.6 GPa could produce a sufficient change in crystal-field configuration to induce a jump in S/T. Magnetic breakdown leads to partial reconstruction of the FS and, consequently, could provide a plausible scenario for the jump in S/T. High field dHvA studies of $CeRhIn_5$, however, are consistent with a lack of evidence for such an effect for fields below 30 T,[21] a field much higher than used in the present study. Though we cannot fully rule out the possibility of magnetic breakdown at p_{c1}, this scenario seems unlikely. Critical valence fluctuations have been proposed theoretically[35] as one explanation for properties of $CeRhIn_5$ at its critical pressure of 2.35 GPa where there is an abrupt jump from small to large FSs. There is, however, no evidence so far as we know from magnetic susceptibility,[26] soft x-ray spectroscopy[33] or resonant X-ray-emission spectroscopy[36] for a valence change across the $Ce(Rh,Ir)In_5$ phase diagram. It again seems very unlikely that a small pressure of 0.61 GPa applied to our sample would induce critical valence fluctuations. Finally, we consider the possibility that a Lifshitz transition might account for transport and thermopower behaviors near p_{c1}. A Lifshitz transition, which does reconstruct the FS, under certain circumstances can produce a jump and sign change in S/T as a function of some non-thermal control parameter that tunes the chemical potential[37] or magnetic exchange.[38] Though these theoretical models[37,38] may capture aspects of our experimental observations, presently it is not possible to compare directly predictions of these models to our results as a function of pressure. In contrast to these plausible interpretations, evidence presented below allows a more straightforward and compelling interpretation of our observations within the framework of quantum criticality.

A model of Kondo-breakdown and SDW QCPs anticipates the behaviors we find around p_{c1} and p_{c2}.[39] This theory predicts a strong increase in S/T as T goes to zero following an $a - bT^{0.5}$ law and that this increase is symmetric about a SDW QCP as it is approached from AFM and paramagnetic states, just as we find at p_{c2} (Fig. 4a,g). We, therefore, identify the magnetic order below T_m as being a spin-density wave. At a Kondo-breakdown QCP, however, S/T should be asymmetric about the QCP (Fig. 4c), in agreement with experimental results at p_{c1} (Fig. 4a). In this theory,[39,40] a sharp peak in S/T on the AFM side of a Kondo-breakdown QCP is expected and signals FS reconstruction. Above the peak, S/T is predicted to follow a $T^{-1/3}$ (2D) or $-\log(T/T_0)$ (3D) temperature dependence. In our case, S/T is better fitted by the latter (cf. Fig. 4e,f). Such a T dependence of S/T also is found in $YbRh_2Si_2$ at $B_c = 65$ mT[41] where an abrupt change in thermopower is accompanied by a field-induced jump in FS, implied from Hall effect measurements, that signals a Kondo-breakdown QCP.[11] We should note that a modified SDW-criticality theory incorporating strong coupling,[42] which predicts $S/T \propto T^{-1/4}$, also fails to describe our results at p_{c1} (Fig. 4e). Though the maximum in S/T at 0.61 GPa is not as sharp as predicted theoretically, some rounding of the

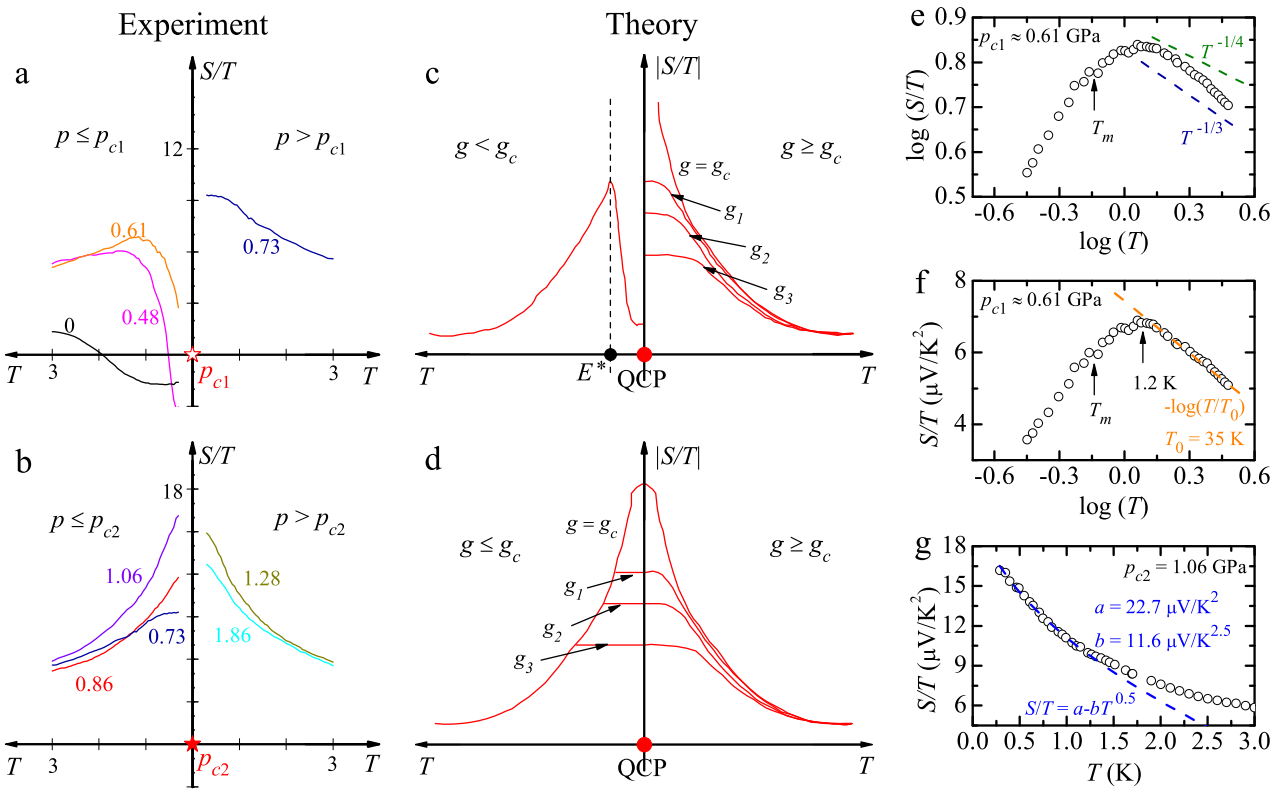

Fig. 4 Thermopower near quantum critical points. **a**–**d** A comparison of *S*/*T* behaviors about a Kondo-breakdown QCP (upper panels) and a SDW QCP (lower panels). The left column shows experimental data (this work), and the right column shows the theoretical predictions reproduced from ref. [39]. In the model calculations, a QCP appears at a critical value of a tuning parameter g_c. Values of g_1, g_2 and g_3 tune the system progressively away from a QCP. Note that theoretical curves are absolute values of *S*/*T*. **e**, **f** plot the temperature-dependent *S*/*T* near p_{c1} and compare it to theoretically predicted dependencies for a Kondo-breakdown QCP as discussed in the text. The dashed line in **f** is a fit to the data above a maximum in *S*/*T*, with the fitting parameters indicated in the figure. **g** *S*/*T* near p_{c2} fitted to the theoretically predicted dependence $a - bT^{0.5}$ expected for a SDW QCP

theoretically sharp feature is expected because of the multi-sheeted FS[28] and the presence of disorder scattering, neither of which is included in this idealized model. Nevertheless, agreement between experiment and theory at both p_{c1} and p_{c2} is appealing (see Fig. 4a–d) and evidence that the two critical points are likely different in nature, p_{c1} being a Kondo-breakdown QCP and p_{c2} a SDW QCP. These results provide an example where two qualitatively different QCPs appear to be realized in a single material driven by a single "clean" tuning parameter that does not break symmetry or induce spin-polarization.

These observations lead us to consider a so-called "global" model of quantum criticality that predicts a sequence of two zero-temperature phase boundaries as a function of some non-thermal tuning parameter,[43–45] which in our case is pressure. Like our experiments in a 9-T field, this model does not consider explicitly the possibility of SC that theoretically can develop from fluctuations around both Kondo-breakdown[46] and SDW[47] critical points. As a function of the tuning parameter, there is in the model a boundary between a magnetically ordered state with small FS (AFM_S) and a SDW state with large FS (AFM_L). As the tuning parameter is increased further, this QCP is followed by another $T = 0$ boundary between SDW and paramagnetic states (PM_L), see Fig. S2 in SI. This sequence of quantum-phase transitions seems to be realized in $CeRh_{0.58}Ir_{0.42}In_5$. Indeed, a more general view of our key observation is that the isothermal *S*/*T*, in the low temperature limit, undergoes a sudden negative-to-positive jump across p_{c1} (Figs. 2f and 4a). This is consistent with a sudden change of the FS from small to large across an unconventional QCP of the Kondo-breakdown type at p_{c1}. We note that *S* at low temperature is negative in $CeRhIn_5$ (data not shown) but positive in $CeIrIn_5$.[48] This change in sign reflects their different electronic structures: in the former, there are three electron FS sheets ($\alpha_{1,2,3}$, band-15) and one hole FS sheet (β_2, band-14),[20] but the latter compound has an additional hole FS sheet (β_1, band-14)[49] as well as larger overall FS.

From the magnetic phase boundaries in Fig. 2d, we also conclude that the FS reconstruction is accompanied by a boundary between large-moment antiferromagnetism and a SDW, as it is in $CeRhIn_5$ at very high magnetic fields.[21] If only part of the FS reconstructs at p_{c1}, it is possible that the SDW manifested at pressures between p_{c1} and p_{c2} is the small-moment, commensurate AFM order at atmospheric pressure that coexists with SC,[24] but if the change in electronic structure is more severe, the SDW at high pressures could be different. Without the possibility of dHvA measurements on $CeRh_{0.58}Ir_{0.42}In_5$, determining the symmetry of the SDW at $p_{c1} \le p \le p_{c2}$ would provide insight on how the Fermi surface changes at p_{c1}. In this regard, it is worth remarking that the transitions to both large-moment incommensurate order and the small-moment commensurate order go to zero simultaneously as a function of *x* in $CeRh_{1-x}Ir_xIn_5$ at atmospheric pressure,[24] unlike the pressure response of $CeRh_{0.58}Ir_{0.42}In_5$.

These models that predict the variation of thermopower around QCPs and the global phase diagram of criticality in heavy-fermion systems are both based on the concept of Kondo breakdown. The theoretically predicted thermopower, however, is for a Kondo-breakdown transition without incorporating any magnetic order.[39,40] This model allows but does not necessarily require criticality of magnetic order simultaneous with a localization/delocalization transition of the *f*-electron and associated jump in

Fermi-surface volume. In contrast, the transition across p_{c1} in pressurized $CeRh_{0.58}Ir_{0.42}In_5$ is between two magnetically ordered phases, as described by the AFM_S-to-AFM_L transition in the global model of criticality (Fig. S2, SI). This suggests that the critical electronic properties of the transition in the magnetic background are indeed dominated by the destruction of Kondo effect. It would be very instructive to carry out similar experiments at a direct transition between AFM_S and PM_L phases, where destruction of the Kondo effect is concurrent with the onset of AFM order; such a setting arises in $CeRhIn_5$ under pressure.[17,20] Thus, our work not only brings new understanding about unconventional quantum criticality but also opens an important means to shed new light on the global phase diagram.

CONCLUSIONS

In summary, pressure-dependent resistivity and thermopower measurements of heavy-fermion $CeRh_{0.58}Ir_{0.42}In_5$ are consistent with two QCPs accessed in a single material with a single clean tuning parameter. As discussed, a straightforward and likely interpretation of experiments is that there is a Kondo-breakdown critical point at $p_{c1} = 0.6$ GPa where the Fermi surface suddenly reconstructs and is accompanied with a transition from large-moment antiferromagnetism to SDW order. This QCP is followed at higher pressures by a SDW QCP at $p_{c2} = 1.06$ GPa beyond which there is a heavy Fermi-liquid state. Thermopower measurements around these critical points provide an experimental manifestation of theoretical predictions. Our work, therefore, also suggests that thermopower can be applicable to detect a Fermi-surface change in other systems when a direct Fermi-surface measurement is not possible. Further, the experimentally established sequence of QCPs and their natures are anticipated in the global phase diagram of heavy-fermion quantum criticality that predicts a series of AFM_S–AFM_L–PM_L transitions at zero-temperature as found in $CeRh_{0.58}Ir_{0.42}In_5$ and depicted in Fig. S2 in SI. It seems likely that the criticality in $CeRh_{0.58}Ir_{0.42}In_5$ generalizes to other members in this series and underlies their SC. These studies uncover systematic insights that should be applicable generally to understanding quantum criticality in heavy-fermion materials and more broadly to bad metals with strong correlations.

METHODS

Single crystalline $CeRh_{0.58}Ir_{0.42}In_5$ was grown from an Indium-rich flux that contained the target ratio of Ce:Rh:Ir.[26,50] The Ir concentration was confirmed by comparing ^{115}In NQR spectra to previous measurements[29] and by energy dispersive x-ray spectroscopy (EDX), both of which gave $x = 0.42(3)$. Though EDX showed that the Ir concentration was highly uniform, we cannot rule out small variations in Rh:Ir ratio throughout the crystal's bulk. Thermopower measurements were carried out by means of a steady-state technique.[48] Both electrical and thermal currents were applied along the *a*-axis that is also the direction of the external magnetic field. Heat capacity under pressure was measured by an AC calorimetric method. A hybrid piston-clamp type cell, with Daphne 7373 as the pressure medium, generated hydrostatic pressures to 2.20 GPa. Pressure in the cell was determined from the SC transition of Pb.

Data availability

The authors declare that all source data supporting the findings of this study are available within the paper.

ACKNOWLEDGEMENTS

We thank T. Park, F. Ronning, J. Lawrence, H. v. Löhneysen, J. Singleton, C. Pépin and L. Jiao for insightful conversations and J. L. Sarrao for providing the sample used in this study. Work at Los Alamos was performed under the auspices of the U.S. Department of Energy, Division of Materials Sciences and Engineering. A. P. Dioguardi and P. F. S. Rosa acknowledge Director's Postdoctoral Fellowships supported through the Los Alamos LDRD program. Work at Rice University was in part supported by the NSF Grant No. DMR-1611392, the ARO Grant No. W911NF-14-1-0525, and the Robert A. Welch Foundation Grant No. C-1411. X. Lu acknowledges the support from National Key R&D Program of China (Grant No. 2017YFA0303101) and National Natural Science Foundation of China (Grant No. 11374257).

AUTHOR CONTRIBUTIONS

Y. L., E. D. B., Q. S. and J. D. T. conceived and designed the experiments. E. D. B., A. P. D. and P. F. S. R. characterized the crystals. Y. L. and X. L. performed the pressure measurements. Y. L., Q. S. and J. D. T. discussed the data, interpreted the results, and wrote the paper with input from all the authors.

ADDITIONAL INFORMATION

Supplementary information accompanies the paper on the *npj Quantum Materials* website (https://doi.org/10.1038/s41535-018-0080-9).

Competing interests: The authors declare no competing financial interests.

Publisher's note: Springer Nature remains neutral with regard to jurisdictional claims in published maps and institutional affiliations.

Change history: A correction to this article has been published and is linked from the HTML version of this article.

REFERENCES

1. Coleman, P. & Schofield, A. J. Quantum criticality. *Nature* **433**, 226–229 (2005).
2. Gegenwart, P., Si, Q. & Steglich, F. Quantum criticality in heavy-fermion metals. *Nat. Phys.* **4**, 186–197 (2008).
3. Sachdev, S. *Quantum Phase Transitions* (Cambridge University Press, Cambridge, UK, 2001).
4. Löhneysen, Hv, Rosch, A., Vojta, M. & Wölfle, P. Fermi-liquid instabilities at magnetic quantum phase transitions. *Rev. Mod. Phys.* **79**, 1015–1075 (2007).
5. Hertz, J. A. Quantum critical phenomena. *Phys. Rev. B* **14**, 1165–1184 (1976).
6. Millis, A. J. Effect of a nonzero temperature on quantum critical points in itinerant fermion systems. *Phys. Rev. B* **48**, 7183–7196 (1993).
7. Schröder, A. et al. Onset of antiferromagnetism in heavy-fermion metals. *Nature* **407**, 351–355 (2000).
8. Custers, J. et al. The break-up of heavy electrons at a quantum critical point. *Nature* **424**, 524–527 (2003).
9. Friedemann, S. et al. Detaching the antiferromagnetic quantum critical point from the Fermi-surface reconstruction in $YbRh_2Si_2$. *Nat. Phys.* **5**, 465–469 (2009).
10. Custers, J. et al. Destruction of the Kondo effect in the cubic heavy-fermion compound $Ce_3Pd_{20}Si_6$. *Nat. Mater.* **11**, 189–194 (2012).
11. Paschen, S. et al. Hall-effect evolution across a heavy-fermion quantum critical point. *Nature* **432**, 881–885 (2004).
12. Luo, Y. et al. Heavy-fermion quantum criticality and destruction of the Kondo effect in a nickel oxypnictide. *Nat. Mater.* **11**, 777–781 (2014).
13. Luo, Y. et al. Pressure-tuned quantum criticality in the antiferromagnetic Kondo semi-metal $CeNi_{2-\delta}As_2$. *Proc. Natl. Acad. Sci. USA* **112**, 13520–13524 (2015).
14. Si, Q., Rabello, S., Ingersent, K. & Smith, J. L. Locally critical quantum phase transitions in strongly correlated metals. *Nature* **413**, 804–808 (2001).
15. Pépin, C. Selective Mott transition and heavy fermions. *Phys. Rev. B* **77**, 245129 (2008).
16. Löhneysen, Hv, Pfleiderer, C., Pietrus, T., Stockert, O. & Will, W. Pressure versus magnetic-field tuning of a magnetic quantum phase transition. *Phys. Rev. B* **63**, 134411 (2001).
17. Park, T. et al. Hidden magnetism and quantum criticality in the heavy fermion superconductor $CeRhIn_5$. *Nature* **440**, 65–68 (2006).
18. Knebel, G., Aoki, D., Braithwaite, D., Salce, B. & Flouquet, J. Coexistence of antiferromagnetism and superconductivity in $CeRhIn_5$ under high pressure and magnetic field. *Phys. Rev. B* **74**, 020501 (2006).
19. Park, T. & Thompson, J. D. Magnetism and superconductivity in strongly correlated $CeRhIn_5$. *New J. Phys.* **11**, 055062 (2009).
20. Shishido, H., Settai, R., Harima, H. & Onuki, Y. A drastic change of the Fermi surface at a critical pressure in $CeRhIn_5$: dHvA study under pressure. *J. Phys. Soc. Jpn.* **74**, 1103–1106 (2005).
21. Jiao, L. et al. Fermi surface reconstruction and multiple quantum phase transitions in the antiferromagnet $CeRhIn_5$. *Proc. Natl. Acad. Sci. USA* **112**, 673–678 (2015).
22. Moll, P. J. W. et al. Field-induced density wave in the heavy-fermion compound $CeRhIn_5$. *Nat. Commun.* **6**, 6663 (2015).

23. Bao, W. et al. Incommensurate magnetic structure of $CeRhIn_5$. *Phys. Rev. B* **62**, R14621–R14624 (2000).
24. Llobet, A. et al. Novel coexistence of superconductivity with two distinct magnetic orders. *Phys. Rev. Lett.* **95**, 217002 (2005).
25. Nicklas, M. et al. Two superconducting phases in $CeRh_{1-x}Ir_xIn_5$. *Phys. Rev. B* **70**, 020505 (2004).
26. Pagliuso, P. G. et al. Coexistence of magnetism and superconductivity in $CeRh_{1-x}Ir_xIn_5$. *Phys. Rev. B* **64**, 100503 (2001).
27. Aso, N. et al. Switching of magnetic ordering in $CeRhIn_5$ under hydrostatic pressure. *J. Phys. Soc. Jpn.* **78**, 073703 (2009).
28. Shishido, H. et al. Fermi surface, magnetic and superconducting properties of $LaRhIn_5$ and $CeTIn_5$ (T: Co, Rh and Ir). *J. Phys. Soc. Jpn.* **71**, 162–173 (2002).
29. Zheng, G.-q et al. Coexistence of antiferromagnetic order and unconventional superconductivity in heavy-fermion $CeR_{h1-}xl_xl_n5$ compounds: nuclear quadrupole resonance studies. *Phys. Rev. B* **70**, 014511 (2004).
30. Knebel, G., Aoki, D., Brison, J. P. & Flouquet, J. The quantum critical point in $CeRhIn_5$: a resistivity study. *J. Phys. Soc. Jpn.* **77**, 114704 (2008).
31. Ziman, J. M. *Principles of the Theory of Solids* (Cambridge University Press, Cambridge, UK, 1972).
32. Behnia, K., Jaccard, D. & Flouquet, J. On the thermoelectricity of correlated electrons in the zero-temperature limit. *J. Phys. Condens. Matter* **16**, 5187–5198 (2004).
33. Willers, T. et al. Correlation between ground state and orbital anisotropy in heavy fermion materials. *Proc. Natl. Acad. Sci. USA* **112**, 2384–2388 (2015).
34. Christianson, A. D. et al. Crystalline electric field effects in $CeMIn_5$(*M*=Co,Rh,Ir): superconductivity and the influence of Kondo spin fluctuations. *Phys. Rev. B* **70**, 134505 (2004).
35. Watanabe, S. & Miyake, K. Origin of drastic change of Fermi surface and transport anomalies in $CeRhIn_5$ under pressure. *J. Phys. Soc. Jpn.* **79**, 033707 (2010).
36. Yamaoka, H. et al. Pressure and temperature dependence of the Ce valence and *c-f* hybridization gap in $CeTIn_5$(*T*=Co,Rh,Ir) heavy-fermion superconductors. *Phys. Rev. B* **92**, 235110 (2015).
37. Buhmann, J. M. & Sigrist, M. Thermoelectric effect of correlated metals: band-structure effects and the breakdown of Mott's formula. *Phys. Rev. B* **88**, 115128 (2013).
38. Kuromoto, Y. & Hoshino, S. Composite orders and lifshitz transition of heavy electrons. *J. Phys. Soc. Jpn.* **83**, 061007 (2014).
39. Kim, K. S. & Pépin, C. Thermopower as a signature of quantum criticality in heavy fermions. *Phys. Rev. B* **81**, 205108 (2010).
40. Kim, K. S. & Pépin, C. Thermopower as a fingerprint of the Kondo breakdown quantum critical point. *Phys. Rev. B* **83**, 073104 (2011).
41. Hartmann, S. et al. Thermopower evidence for an abrupt Fermi surface change at the quantum critical point of $YbRh_2Si_2$. *Phys. Rev. Lett.* **104**, 096401 (2010).
42. Abrahams, E. & Wölfle, P. Critical quasiparticle theory applied to heavy fermion metals near an antiferromagnetic quantum phase transition. *Proc. Natl. Acad. Sci. USA* **109**, 3238–3242 (2012).
43. Si, Q. Global magnetic phase diagram and local quantum criticality in heavy fermion metals. *Phys. B* **378–380**, 23–27 (2006).
44. Coleman, P. & Nevidomskyy, A. H. Frustration and the Kondo effect in heavy fermion materials. *J. Low. Temp. Phys.* **161**, 182–202 (2010).
45. Nica, E. M., Ingersent, K. & Si, Q. Quantum criticality and global phase diagram of an Ising-anisotropic Kondo lattice. Preprint at https://arxiv.org/abs/1603.03829 (2016).
46. Pixley, J. H., Deng, L., Ingersent, K. & Si, Q. Pairing correlations near a Kondo-destruction quantum critical point. *Phys. Rev. B* **91**, 201109(R) (2015).
47. Monthoux, P., Pines, D. & Lonzarich, G. G. Superconductivity without phonons. *Nature* **450**, 1177 (2007).
48. Luo, Y., Rosa, P. F. S., Bauer, E. D. & Thompson, J. D. Vortexlike excitations in the heavy-fermion superconductor $CeIrIn_5$. *Phys. Rev. B* **93**, 201102 (2016).
49. Haga, Y. et al. Quasi-two-dimensional Fermi surfaces of the heavy fermion superconductor $CeIrIn_5$. *Phys. Rev. B* **63**, 060503 (2001).
50. Petrovic, C. et al. A new heavy-fermion superconductor $CeIrIn_5$: a relative of the cuprates? *EPL* **53**, 354C359 (2001).